Radio Science from an Optical Communications Signal

Bruce Moision, Sami Asmar, Kamal Oudrhiri
Jet Propulsion Laboratory
California Institute of Technology
Pasadena, CA 91109-8099
Bruce.Moision@jpl.nasa.gov, Sami.Asmari@jpl.nasa.gov, Kamal.Oudrhiri@jpl.nasa.gov,

***Abstract*—NASA is currently developing the capability to deploy deep space optical communications links. This creates the opportunity to utilize the optical link to obtain range, doppler, and signal intensity estimates. These may, in turn, be used to complement or extend the capabilities of current radio science. In this paper we illustrate the achievable precision in estimating range, doppler, and received signal intensity of an non-coherent optical link (the current state-of-the-art for a deep-space link). We provide a joint estimation algorithm with performance close to the bound. We draw comparisons to estimates based on a coherent radio frequency signal, illustrating that large gains in either precision or observation time are possible with an optical link.**

TABLE OF CONTENTS

1 INTRODUCTION 1
2 PARAMETER ESTIMATION FOR A DIRECT-DETECTED OPTICAL SIGNAL 2
3 JOINT PARAMETER ESTIMATION 4
4 COMPARISON WITH ESTIMATION FROM A COHERENTLY RECEIVED RF SIGNAL 4
5 CONCLUSIONS/DISCUSSION 6
REFERENCES 7
BIOGRAPHY 7

1. INTRODUCTION

The Jet Propulsion Laboratory (JPL) is currently developing technology to support optical communications with spacecraft in deep-space. A deep-space optical communications link can support orders of magnitude larger data rates than its radio-frequency (RF) counterpart for the same terminal mass and power [1], [2]. The optical link may also be used to derive range and doppler estimates, much as its RF counterpart. We would expect that estimates of these parameters would similarly see improvements in accuracy relative to the RF case.

A complete ranging protocol must take into account errors accumulated at many layers, including calibration errors, relative-timing errors, parameter estimation errors, etc. In this paper we will concentrate exclusively on the physical layer, specifically, on the parameter estimation accuracy of a one-way-link of the ranging system. Our analysis in this paper quantifies the performance improvement that may be gained by estimating parameters of an intensity modulated optical signal, rather than those of a pure microwave-frequency tone, and provides an intuitive comparison of the physical signal characteristics governing the accuracy in the two cases. Hence our results address the gains in one component of the error budget governing a complete ranging system.

Optical links in development at JPL utilize intensity-modulation, noncoherent photon-counting receivers, and carriers in the infrared regime, from 2.1 to 2.6 μm [1]. These choices are made to maximize the power efficiency of the link and take into account constraints of current technology. In this paper, we consider deriving measurements from this optical telemetry link. Throughout we use the shorthand 'optical' to refer to an intensity-modulated infrared signal received with a noncoherent photon-counting receiver. We determine the accuracy with which one may measure phase, frequency, and intensity of an optical signal. We extend prior work on individual estimators in [3] to joint estimators, deriving the joint Cramèr-Rao-Bounds (CRBs) and proposing a joint estimator with error close the to bounds.

We compare the optical estimates to the conventional state-of-the-art estimation from coherently demodulated microwave, or radio-frequency (RF), carriers. Conventional RF science is derived from a ranging clock, which may be modeled as a sinusoid received in AWGN, see, e.g., [4, Chapter 3],

$$y)t+\mathrm{B}\ A\,\mathrm{dpt}\,)3\pi f_r t \quad \phi+0\ \ n)t+ \tag{1}$$

where A is the signal amplitude, f_r is the range clock frequency, ϕ is the phase, and $n)t+$is additive white Gaussian noise. An example is illustrated in Figure 1 for f_r B 2 MHz. Estimating the instantaneous phase, frequency, and amplitude of the RF waveform allows one to determine properties of processes that distort these parameters. For example, spacecraft range may be determined from the transmitter delay, via an estimate of the phase, and velocity determined by the induced doppler shift, via an estimate of the frequency. Analogous properties of the signal waveform may be extracted from the photocurrent generated from an intensity-modulated optical signal incident on a photon-counting detector. The photocurrent, when normalized by the electron charge, is modeled as a random Poisson point process, governed by a rate function

$$l)t+\mathrm{B}\ l_p \int_{k=-\infty}^{\infty} \rho)t \quad kT_r \quad \phi'+0\ \ l_b \tag{2}$$

where l_p denotes the peak photo-electron rate in pe/sec, $\rho)t+$ is the intensity pulse shape, satisfying $2 \approx \rho)t+\approx 1$, T_r is the repetition period, ϕ' is the phase, and l_b is the mean photo-electron rate from other sources, such as thermal[2] and dark noise [3]. Figure 2 illustrates an example rate function and

©2012 California Institute of Technology. Government sponsorship acknowledged. This research was carried out at the Jet Propulsion Laboratory, California Institute of Technology, under a contract with the national Aeronautics and Space Administration.
978-1-4577-0557-1/12/$26.00 ©2012 IEEE.
[1] IEEEAC Paper #2438, Version 1, Updated 10/29/2012.

[2] We assume thermal noise is multi-mode with sufficient number of modes to justify a Poisson approximation
[3] Although dark noise does not, strictly speaking, generate photo-electrons, for convenience we utilize units of photo-electrons for all electrons.

a realization of a random point process, representing photo-electron arrivals, induced by it. Analogous to the parameter estimates obtained from an RF carrier, we may estimate l_p, T_r, and ϕ, based on observing photo-electron emissions governed by the rate function $l)t+$.

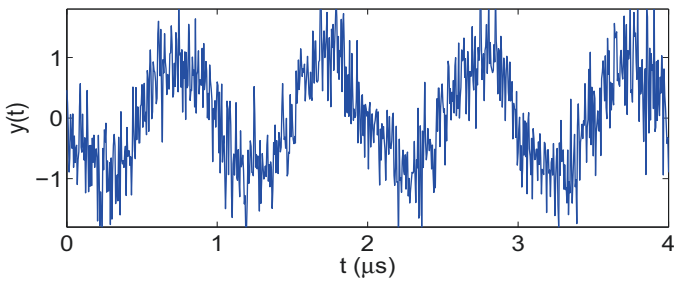

Figure 1. Coherent Microwave (RF) Received Signal

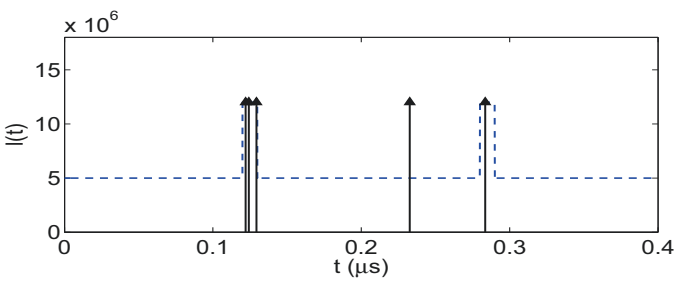

Figure 2. Noncoherent Infrared (Optical) Received Signal

The paper is organized as follows. In Section 2, we establish a model and general framework for studying the problem, and derive the CRBs. In Section 3 we formulate a candidate joint estimation algorithm. In Section 4 we review the analogous results for the RF signal and draw comparisons utilizing parameters for current state-of-the art links. In Section 5 we briefly discuss the results.

2. Parameter Estimation for a Direct-Detected Optical Signal

In any implementation of a parameter estimation system, many errors contribute to the overall performance, such as clock drift, clock offset, transmitter and detector jitter, and calibration. Here we determine the estimation error for a one-way link, limited only by the received signal and noise powers and observation times, and otherwise ideal.

Channel Model

We model the received signal as follows. A periodic repeating optical pulse train is transmitted in vacuum. At the receiver, the light is focused on an ideal photodetector. The ideal detector has negligible thermal noise, and sufficient bandwidth that individual photon arrival times may be observed at its output. The output is a random photocurrent, which, normalized by the electron charge, is accurately modeled as an inhomogeneous Poisson process with rate function given by (2).

The signal parameters are determined by the underlying communications link, which we presume is implemented with pulse-position-modulation (PPM), wherein time is divided into slots of duration T_s, with T_s on the order of the pulse width. It is convenient, in this context, to normalize time to be in units of slots[4], that is, defining

$$u \overset{\text{def}}{\text{B}} t/T_s\,, \tag{3}$$

the rate function of the inhomogenous Poisson process that describes the photocurrent is expressed as

$$(\ )u+\overset{\text{def}}{\text{B}}\ T_s l)uT_s+\text{B}\ n_s \int_{k=-\infty}^{\infty} g)u \quad kT \quad \phi+0\ \ n_b\,, \tag{4}$$

where $n_s \overset{\text{def}}{\text{B}} l_p \sum g)t+et$ is the mean signal photo-electrons per pulse, $n_b \overset{\text{def}}{\text{B}} l_b T_s$ is the mean number of noise photo-electrons per slot, $T \overset{\text{def}}{\text{B}} T_r/T_s$ is the repetition period in slots, ϕ B ϕ'/T_s is the phase of the periodic waveform, and

$$g)u+\text{B}\ \frac{f)uT_s+}{\sum f)uT_s+eu} \tag{5}$$

is the normalized pulse shape. We assume a generalized Gaussian pulse,

$$g)u+\text{B}\ \frac{p}{3a\ \ )2/p+}\text{g}\tilde{}\text{r})\ \ \underset{\surd}{u}/a\ \underset{\surd}{p}+, \tag{6}$$

where $)\leq+$ is the Gamma function, a is the $2/e$ width of the pulse, and p is the decay rate of the pulse tails. Figure 3 illustrates the pulse for a range of values of p. Throughout, for convenience, we assume p is an even integer. This parameterized pulse shape models a wide range of practical pulse shapes, from Gaussian (p B 3), to square (large p, e.g., p B 21 or greater).

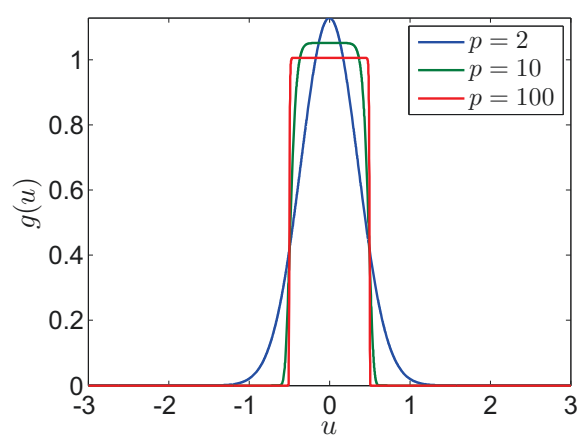

Figure 3. Generalized Gaussian pulse shapes for several decay rates p.

Cramèr Rao Bounds

We treat the problem of estimating n_s, T and ϕ. We assume throughout that the unknown parameters are constant over the observation period. We also assume that the noise mean n_b is known[5]. Estimates are based on the observation of photon arrivals over an interval of duration T_i B KT. Suppose

[4]Note that this normalization is simply a unit conversion to units of time in slotwidths at the receiver. This is done to simplify notation and make it easier to generalize results, but does not imply the receive has knowledge of the slotwidth.

[5]The noise mean is typically slowly time varying, and may be estimated with an accuracy justifying this assumption.

that we observe N arrivals at times $\}u_1, u_2, \ldots, u_N|$. The conditional log joint density of the collection of observations is [5]

$$\begin{aligned} &\text{mpi } p)\}u_i|\,, N+\text{B} \\ &\sum \quad \sum_{T_i}(\ )u+\text{e}\,u\ 0\ \int_{i=0}^{N-1} \text{mpi } (\ )u_i+ \qquad \text{,for } N > 1 \\ &\qquad \sum_{T_i}(\ )u+\text{e}\,u \qquad\qquad\qquad\qquad \text{,for } N \text{ B } 1. \end{aligned} \tag{7}$$

Let θ B $]\phi, T, n_s\hat{}$, the vector of parameters we are estimating. The Cramèr-Rao Bound (CRB), which bounds the variance of an unbiased parameter estimate, is given by

$$\text{FS C}_{\theta_i} \text{ B }]I)\theta+^{-1}|_{i,i} \tag{8}$$

where $I)\theta+$is the Fisher information matrix

$$]I)\theta+\hat{}_{i,j} \text{ B } \quad E\Big]\frac{\partial^2 \text{ mn } p)\}u_i|\,, N+}{\partial\theta_i\partial\theta_j}\Big(\tag{9}$$

We have

$$\begin{aligned} &\frac{\partial^2 \text{ mpi } p)\}u_i|\,, N+}{\partial\theta_i\partial\theta_j}\text{B} \\ &\quad \sqrt{_{T_i}} \frac{\partial^2(\ )u+}{\partial\theta_i\partial\theta_j}du\ 0\ \int_{i=0}^{N-1} \frac{2}{(\ )u_k+}\frac{\partial^2(\ )u+}{\partial\theta_i\partial\theta_j} \\ &\frac{2}{(\ ^2)u_k+}\frac{\partial(\ )u_k+}{\partial\theta_i}\frac{\partial(\ )u_k+}{\partial\theta_j} \end{aligned} \tag{10}$$

Let $\{ \ )u+$denote the (random) counting process induced by $(\ )u+$, and $i)t+$B $d\{ \ )u+/du$–in our case, the resulting normalized photo-current (a sum of discrete photo-electrons). Note that

$$E)i)u++\text{B } (\ )u+ \tag{11}$$

Let $h)u+$be some deterministic function of u. Note that

$$\int_i h)u_i+\text{B } \sqrt{i)u+}h)u+du \tag{12}$$

$$E\Big]\int_i h)u_i+\Big\{\text{B } \sqrt{(\ )u+}h)u+du \tag{13}$$

Applying this to (10) yields

$$]I)\theta+\hat{}_{i,j} \text{ B } \sqrt{_{T_i}} \frac{2}{(\ )u+}\frac{\partial(\ )u+}{\partial\theta_i}\frac{\partial(\ )u+}{\partial\theta_j}du \tag{14}$$

Consider the $)n_s, \phi+$term in $I)\theta+$. We have

$$\frac{\partial(\ )u+}{\partial\phi}\text{B } \frac{n_s p}{a^p}\int_{k=-\infty}^{\infty} g)w+)w+^{p-1} \tag{15}$$

$$\frac{\partial(\ )u+}{\partial n_s}\text{B } \int_{k=-\infty}^{\infty} g)w+ \tag{16}$$

$$\begin{aligned} &]I)\theta+\hat{}_{n_s,\phi} \text{ B} \\ &\quad \frac{n_s p}{a^p}\sqrt{_{T_i}} \frac{\int_{\ k} g)w+w^{p-1}\int_{\ k} g)w+}{n_s\int_{\ k} g)w+0\ \ n_b}du \end{aligned} \tag{17}$$

where, for concise representation, we put w B $u \quad kT \quad \phi$. We assume pulses are non-overlapping. That is, that $g)u+g)u \quad kT+\gg 1$ for all u for k B N 1. Since the pulse tails decay exponentially, while $w^{(p-1)}$ grows polynomially, the cross terms in the numerator are negligible. Similarly, only the corresponding term (the pulse with the same shift) in the denominator has a significant contribution. Hence

$$]I)\theta+\hat{}_{n_s,\phi} \gg \int_{b=0}^{K-1} \frac{n_s p}{a^p}\sqrt{_{v=-\infty}^{\infty}} \frac{g^2)v+w^{p-1}}{n_s g)v+0\ \ n_b}dv \tag{18}$$

$$\text{B } 1 \tag{19}$$

which evaluates to zero since the integrand is an odd function.

Consider the $)\phi, T+$term in $I)\theta+$. Similarly, we have

$$\frac{\partial(\ )u+}{\partial T}\text{B } \frac{n_s p}{a^p}\int_{k=-\infty}^{\infty} kg)w+)w+^{p-1} \tag{20}$$

$$]I)\theta+\hat{}_{\phi,T} \gg\Big)\frac{n_s p}{a^p}\Big(^2\int_{b=0}^{K-1} k\sqrt{_{v=-\infty}^{\infty}} \frac{g^2)v+w^{2(p-1)}}{n_s g)v+0\ \ n_b}dv \tag{21}$$

where the approximation follows, as with the prior argument, for non-overlapping pulses. In this paper, we will be interested in the case $n_s g)1+/ \ \ n_b$, i.e., the high signal-to-noise ratio regime. Under this assumption we have

$$]I)\theta+\hat{}_{\phi,T} \gg\Big)\frac{n_s p}{a^p}\Big(^2\frac{K)K \quad 2+}{3}\sqrt{_{v=-\infty}^{\infty}} g)v+w^{2(p-1)}dv \tag{22}$$

$$\text{B } \frac{K)K \quad 2+n_s p^2 \ \ )3 \quad 2/p+}{3a \ \ )2/p+} \tag{23}$$

By a similar analysis with the remaining terms, we have

$$]I)\theta+\hat{}_{n_s,n_s} \gg \frac{K}{n_s} \tag{24}$$

$$]I)\theta+\hat{}_{\phi,\phi} \gg \frac{Kn_s p}{a^2} \tag{25}$$

$$]I)\theta+\hat{}_{T,T} \gg \frac{K^3 p^2 \ \ )3 \quad 2/p+n_s}{4a^2 \ \ )2/p+} \tag{26}$$

$$]I)\theta+\hat{}_{n_s,T} \gg 1 \tag{27}$$

It is straightforward to invert the Fisher information matrix. In doing so, we obtain terms that are quadratic in K. Our region if interest is in large K. Taking the K^2 terms yields the asymptotic (large K) CRBs

$$\text{FS C}_T \gg \kappa\frac{4a^2 \ \ )2/p+}{K^3 n_s p^2 \ \ )3 \quad 2/p+} \tag{28}$$

$$\text{FS C}_\phi \gg \kappa\frac{a^2}{Kn_s p} \tag{29}$$

$$\text{FS C}_{n_s} \gg \frac{n_s}{K} \tag{30}$$

where

$$\kappa \text{ B } \frac{2}{2 \quad \frac{3pa^2\Gamma(2-1/p)}{4\Gamma(1/p)}} \tag{31}$$

We've factored CRB_ϕ and CRB_T into the product of the CRB of the individual estimator-that is, the CRB when the other terms are known-times a loss term κ. The loss term depends only on the pulse shape via the parameters $)a, p+$. Hence, the loss due to not knowing the other parameters is a fixed constant that depends only on the pulse shape. The signal photon number CRB is identical to the individual CRB.

3. JOINT PARAMETER ESTIMATION

In this section we develop a joint estimator for $]\phi, T, n_s\hat{}$ that has performance close the to CRB. The estimator is formed by iterating between the individual parameter maximum-likelihood (ML) estimators.

Phase

Given estimates $)\hat{T}, \hat{n}_s+$ of the period and signal rate, we estimate the phase as

$$\hat{\phi} \text{ B csi n c}\tilde{}_{\tilde{\phi}} \int_{j=0}^{N-1} \text{mpi}\Big)\hat{n}_s g\ ]u_i \quad \phi\hat{}_{\hat{T}}\big[\ 0\ n_b\Big(, \tag{32}$$

where $]u\hat{}_T \overset{\text{def}}{\text{B}})u\ 0\ T/3\ \text{n pe}\ T+\ T/3$. This is the approximate ML phase estimate if $\hat{T} \text{ B } T, \hat{n}_s \text{ B } n_s$ [3].

Intensity

The ML estimate of the intensity with $)T, \phi+$known $\hat{n}_{s,\text{ML}}$, satisfies

$$\int_{j=0}^{N-1} \frac{g)u_i \quad \phi+}{\hat{n}_{s,\text{ML}} g)u_i \quad \phi+0\ n_b} \gg K \tag{33}$$

If we approximate the pulse as uniform on $]\ \beta, \beta+$and zero otherwise, we have the approximation

$$\hat{n}_{s,\text{ML}} \gg \frac{2}{K} N_{[-\beta,\beta]} \quad 3\beta n_b \tag{34}$$

where $N_{[t_1,t_2]}$ is the number of arrivals on $]t_1, t_2\hat{}$. Estimate (34) is the number of arrivals over an approximate pulse duration, minus the mean noise arrivals on the same period. However, if the phase is not known in the $n_s g)1+/\ n_b$ regime, an accurate estimate of n_s can be formed by simply dividing the number of arrivals by the estimated number of pulses

$$\hat{n}_s \text{ B } \frac{N_{[0,T_i]}}{\hat{K}} \quad 3\beta n_b \tag{35}$$

where $\hat{K} \text{ B } T_i/\hat{T}$.

Period

Given estimates $)\hat{n}_s, \hat{\phi}+$, we estimate the period as

$$\hat{T} \text{ B csi n c}\tilde{}_{\tilde{T}} \quad \hat{n}_s K\ 0 \int_{j=0}^{N-1} \text{mpi}\ )\hat{n}_s g)]u_i \quad \hat{\phi}\hat{}_{\tilde{T}}+0\ n_b+ \tag{36}$$

This is the approximate ML period estimate when $\hat{n}_s \text{ B } n_s, \hat{\phi} \text{ B } \phi$ [3]. We find the maximum of (36) numerically, using a grid search around a region of the true value. In doing so, we assume prior knowledge of the parameter domain. This is a valid assumption as the period will be known within a range bounded by uncertainties due to transmitter clock stability and Doppler predicts.

Joint Estimator

As suggested above, the joint estimator is formed by iterating between the individual estimators, each given by the ML estimator with the current estimates of the other parameters. To initialize, we first obtain an estimate of the period by setting $\hat{\phi} \text{ B } 1, \hat{n}_s \text{ B } 1$ in $\hat{T}$. We then estimate n_s via (35), and iterations proceed by evaluating $\hat{\phi}, \hat{T}, \hat{n}_s, \ldots$, at each step setting inputs $)\phi, T, n_s+$to their current estimate.

Unit Conversion

In the following section we draw comparisons to the estimation errors for an RF signal. To draw comparable conclusions, we convert the phase, period, and photon-number estimates to range, (normalized)frequency, and (normalized)power, respectively. To do so, we assume the path time-of-flight, $\Lambda t \text{ B } AT\ 0\ \phi$, is known a-priori to within one period (A is known, and $\phi \geq T$ [6]), and the transmission path is vacuum. This yields range, frequency, and power estimates:

$$r \text{ B } c\Lambda t\ )m+ \tag{37}$$

$$f \text{ B } 2/)TT_s+)\text{Hz}+ \tag{38}$$

$$P_r \text{ B } \frac{n_s hc}{TT_s\lambda}\ )W+ \tag{39}$$

where h is Planck's constant, c is the speed of light in vacuum, and λ is the carrier wavelength. It is a straightforward exercise to convert the RMS estimator errors and CRBs from phase, period, and photon-number, to the corresponding errors and bounds on range, frequency, and power.

4. COMPARISON WITH ESTIMATION FROM A COHERENTLY RECEIVED RF SIGNAL

As discussed earlier, the received RF ranging signal may be modeled as a sinusoid in additive white Gaussian noise

$$y)t+\text{B } A\,\text{dpt}\ )3\pi f_r t\ 0\ \phi+0\ n)t+ \tag{40}$$

where A is the signal amplitude ($A \text{ B } \sqrt{3P_r}$ where P_r is the received power in the range signal), f_r is the range clock frequency, and ϕ is the phase. The additive noise $n)t+$is Gaussian noise with power spectral density $S_n)f+\text{B } N_0/3$ Watts/Hz on $]\ W, W\hat{}$ and zero elsewhere. The signal is sampled at rate $f_s \text{ B } 3W$. Put $f_0 \text{ B } f_r/f_s$. Estimates are based on a collection of N samples

$$y_n \text{ B } A\,\text{dpt}\ )3\pi f_0 n\ 0\ \phi+0\ w_n \tag{41}$$

where w_n is an IID, zero-mean, Gaussian sequence with variance $\sigma^2 \text{ B } WN_0$. Approximate ML estimates and the CRBs for estimating $)f_0, A, \phi+$are well known, see, e.g., [6].

[6]The notion of the period may been to be increased by sending a pseudo-random sequences of pulses to make this a valid assumption

We simply restate the results here:

$$\mathrm{FSC}_{f_0} \gg \frac{7\sigma^2}{A^2\pi^2N^3} \tag{42}$$

$$\hat{f}_{0ML} \gg \mathrm{csi\ n\ c}_{\tilde{f}_0}\left(\sum_{n=0}^{N-1} y_n\,\mathrm{g\tilde{r}}\right) \quad j3\pi f_0 n+ \tag{43}$$

$$\mathrm{FSC}_A \ \mathrm{B}\ \frac{3\sigma^2}{N} \tag{44}$$

$$\hat{A}_{ML} \gg \frac{3}{N}\left(\sum_{n=0}^{N-1} y_n\,\mathrm{g\tilde{r}}\right)3\pi\hat{f}_{0ML}n+ \tag{45}$$

$$\mathrm{FSC}_\phi \ \mathrm{B}\ \frac{9\sigma^2}{NA^2} \tag{46}$$

$$\hat{\phi}_{ML} \gg \mathrm{csdxco}\left(\frac{\int_{n=0}^{N-1} y_n\,\mathrm{tlo})3\pi\hat{f}_{0ML}n+}{\int_{n=0}^{N-1} y_n\,\mathrm{dpt})3\pi\hat{f}_{0ML}n+}\right. \tag{47}$$

Table 1 compares the achievable RMS errors (RMS B $\overline{\mathrm{MSE}} \approx \quad \mathrm{FSC}$), or normalized versions, for ideal RF and optical links (recall we use the high signal power asymptotes for the optical case). We see similar behavior for each parameter. The RMS phase error is inversely proportional to the product of the power and the integration time, the frequency error is inversely proportional to the product of the power and the cube of the integration time, and the intensity error goes as the power on the integration time. Hence the slopes of RMS error versus either integration time or SNR will be the same for RF and optical. In order to compare performance requires a determination of the signal and noise powers, which we treat for a sample pair of links in the next section.

Representative Link Budgets for a Mars-Earth Downlink

In this section we compare two specific candidate Mars-Earth downlinks: a Ka-band RF link with carrier frequency 43 GHz (wavelength =4 mm), and an optical link in the near-infrared with carrier frequency 2=4.6 THz (wavelength 2.66 μm). The link budgets are provided in Table 2. The Ka-band link parameters are chosen to correspond to a Ka-band Mars-Reconnaissance-Orbiter link [7], [8]. The optical link parameters are chosen to correspond to the Deep-Space-Optical Transceiver (DOT) concept [1]. The DOT concept was designed to have comparable mass and power as the Ka-band terminal. Hence the comparison is normalized for comparable burden on the spacecraft terminal. These represent current state-of-the-art candidates for a deep-space telecommunications link.

For the optical link, we assume a receive telescope diameter D_r B 22.9 m, corresponding to the Large Binocular Telescope in southeastern Arizona. We choose T_s B 1.53 ns, a target slotwidth at a range of 1.53 AU. To be conservative, we choose a worst case noise power for this link, P_n B 4.39 r[[1]. At long integration times, the noise is negligible, reflected in the large signal power CRBs. From these parameters, we find the received power from the link equation

$$P_r \ \mathrm{B}\ P_t\Big)\frac{\pi D_t D_r}{5R\lambda}\Big[^2\ \eta \tag{48}$$

where R is the range and λ the carrier wavelength. From the link budgets we obtain

$$n_s \ \mathrm{B}\ \frac{P_r T T_s \lambda}{hc} \ \mathrm{B}\ 2.=6 \quad)\mathrm{pe/pulse+} \tag{49}$$

$$n_b \ \mathrm{B}\ \frac{P_n \lambda T_s}{hc} \ \mathrm{B}\ 1.12 \quad)\mathrm{pe/slot+} \tag{50}$$

For the RF link, we assume a receive antenna diameter D_r B 45 m, corresponding to a Deep Space Network antenna. We assume a range clock modulation index of 1.9 rad, hence the received power is [9]

$$P_r \ \mathrm{B}\ P_t\Big)\frac{\pi D_t D_r f_c}{5Rc}\Big[^2\ \eta 3J_1^2) \quad \bar{3}\phi_r+ \tag{51}$$

where J_1 is a Bessel function of the first kind or order 2. From the link equation we obtain

$$A^2 \ \mathrm{B}\ 3P_r \ \mathrm{B}\ 1.16 \quad)\mathrm{pW+} \tag{52}$$

$$\sigma^2 \ \mathrm{B}\ N_0 W \ \mathrm{B}\ 1.113 \quad)\mathrm{pW+} \tag{53}$$

Ka-band Link		
f_0	carrier frequency	43.1 GHz
f_r	range clock	2.1 MHz
ϕ_r	range mod. index	1.9 rad
ϕ_c	data mod. index	1.1 rad
D_t	transmit diameter	4.1 m
D_r	receiver diameter	45.1 m
η	system efficiency	21 dB
N_o	noise spectral density	289.56 dB-mW/Hz
W	bandwidth	2.6 MHz
P_t	transmit power	46 W

Near-Infrared Link		
λ	wavelength	2.66 μm
D_t	transmit diameter	33.1 cm
D_r	receiver diameter	22.9 m
η	system efficiency	27.85 dB
α_b	noise spatial density	1.14 pW/n ^{2}
T_s	slot width	1.53 ns
p	pulse shape	3
a	pulse width	2/3
M B T	PPM order	27
P_t	transmit power	5 W

Table 2. Sample Ka-band and Infrared Link Parameters

Estimator Performance

Figures 4, 5, and 6 illustrates the CRBs for the operating points in Table 2, along with the performance of the two joint estimators described earlier: the (approximate) joint-ML RF estimator, and the iterative optical estimator. We see that the optical power estimate is robust, as we would expect, and that joint optical estimation of frequency and phase performs close to the CRB.

Since the errors behave the same as a function of the integration time, we see the difference in the RMS errors may be factored into three constituent terms: a ratio of received powers, a ratio of noise contributions, and a ratio of the bandwidths of the signals. The ratio of the square of the received power for our presumed budgets is 27 dB. This is a result of the large divergence gain when transmitting at

	RMS error	
parameter	pr xldcm	S M
S R W$_{\text{range}}$)m+	$c\ \overline{\Big)\frac{2}{T_iP_r}\Big[\ \Big)\frac{hc}{\lambda}\Big[\ \Big)\frac{a^2T_s^2\kappa}{p}\Big[}$	$c\ \overline{\Big)\frac{2}{T_iP_r}\Big[\ )3N_0+\Big)\frac{2}{)3\pi f_r+^2}\Big[}$
$\frac{\text{S R W}_f}{f}$	$\overline{\Big)\frac{2}{T_i^3P_r}\Big[\ \Big)\frac{hc}{\lambda}\Big[\ \frac{4)aT_s+^2\ \ )2/p+\kappa}{p^2\ \ )3\ \ \ 2/p+}}$	$\overline{\Big)\frac{2}{T_i^3P_r}\Big[\ )3N_0+\Big)\frac{4}{)3\pi f_r+^2}\Big[}$
$\frac{\text{S R W}_{P_r}}{P_r}$	$\overline{\Big)\frac{2}{P_rT_i}\Big[\ \Big)\frac{hc}{\lambda}\Big[}$	$\overline{\Big)\frac{2}{P_rT_i}\Big[\ )3N_0+}$

Table 1. Comparison of achievable parameter estimation accuracies in the high SNR regime. h is Planck's constant and c the speed of light in vacuum.

optical wavelengths. The ratio of the noise contributions relates the shot noise of the optical signal to the thermal noise of the RF signal. As we have factored the terms, this benefits the RF signal by approximately 9 dB. The final term is the ratio of the signal features, or bandwidth, which appears as $)aT_s5\pi f_r+^2/p$ (note that for p B 3, the ratios of the constants is the same). For our signals, this ratio is approximately 3= dB. Hence we see gains on the order of 48 dB for range and fractional frequency estimates, and on the order of 9 dB for the power estimate, which doesn't benefit from the bandwidth gain.

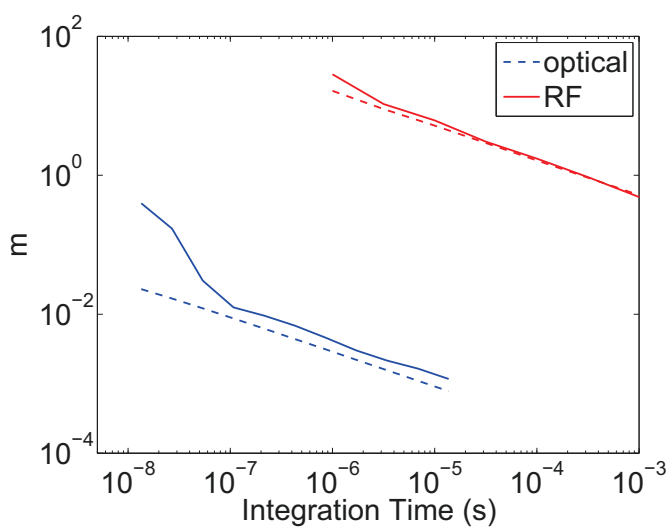

Figure 4. Achievable RMS Range Error $)m+$for Example RF and Optical One-Way Links. Solid line is the estimator performance, dashed is the CRB asymptote.

5. Conclusions/Discussion

In this paper we derived the CRBs and a candidate estimator for joint estimation of the phase, period, and intensity of a direct-detected intensity-modulated (optical) signal. We illustrated that the joint CRBs of phase and period are degraded from the individual CRBs by a constant that depends only on the pulse shape. We demonstrated the performance of an iterative estimator with performance close to the CRBs. In

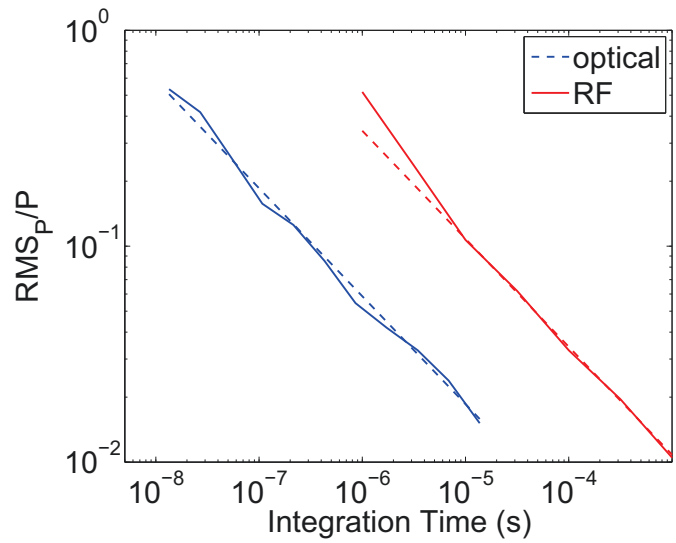

Figure 5. Achievable Fractional RMS Power Error for Example RF and Optical One-Way Links. Solid line is the estimator performance, dashed is the CRB asymptote

comparing the optical CRBs to those for the RF case, we see the forms are analogous in their dependence on the integration time, signal power, noise power, and bandwidth, where the RF analog of shot noise (photon energy) is N_0, and the RF analog of bandwidth (the reciprocal of the pulsewidth for optical) is the range clock frequency. Hence the performance difference between optical and RF systems comes down to the realization of these parameters. We provided a sample comparison for sets of parameters taken from mass-and-power normalized spacecraft terminals, illustrating several orders of magnitude gain improvement in the CRBs for the optical system over its RF counterpart. This addresses only one aspect of a full ranging system. A complete comparison will have to look at all error sources, including joint estimator of unknown parameters, and resolution of the period ambiguity, in a full, round-trip, ranging protocol.

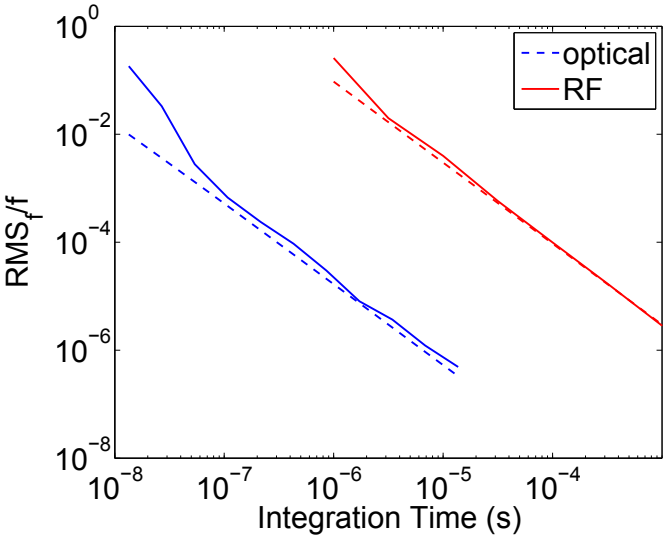

Figure 6. Achievable Fractional RMS Frequency Error for Example RF and Optical One-Way Links. Solid line is the estimator performance, dashed is the CRB asymptote.

REFERENCES

[1] A. Biswas, H. Hemmati, S. Piazzolla, B. Moision, K. Birnbaum, and K. Quirk, "Deep-space optical terminals (DOT) systems engineering," *IPN Progress Report*, vol. 42–183, November 2010.

[2] W. D. Williams, M. Collins, D. M. Boroson, J. Lesh, A. Biswas, R. Orr, L. Schuchman, and O. S. Sands, "RF and optical communications: A comparison of high data rate returns from deep space in the 2020 timeframe," NASA/TM, Tech. Rep. 2007-214459, March 2007, available at `http://gltrs.grc.nasa.gov`.

[3] B. E. Moision and B. I. Erkmen, "Bounds on parameter estimation precision for optical ranging systems," in *Proceedings of the SPIE*, San Diego, CA, October 2012.

[4] J. H. Yuen, Ed., *Deep Space Telecommunications Engineering*. New York: Plenum Press, 1983, ch. Receiver Design and Performance Characteristics.

[5] D. L. Snyder, *Random Point Processes*. Wiley, 1975.

[6] S. M. Kay, *Fundamentals of Statistical Signal Processing: Estimation Theory*. Prentice Hall, 1993.

[7] W. D. Williams, M. Collins, R. Hodges, R. S. Orr, O. S. Sands, L. Schuchman, and H. Vyas, "High-capacity communications from Martian distances," NASA/TM, Tech. Rep. 2007-214415, December 2007, available at `http://gltrs.grc.nasa.gov`.

[8] S. Shambayati, D. Morobito, J. S. Broder, F. Davarian, D. Lee, R. Mendoza, M. Britcliffe, and S. Weinreb, "Mars Reconnaissance Orbiter Ka-band (32 GHz) demonstration: Cruise phase operations."

[9] P. W. Kinman and J. B. Berner, "Two-way ranging during early mission phase," ser. Proceedings of the IEEE Aerospace Conference, March 2003.

BIOGRAPHY

Bruce Moision received his B.S. in Engineering from Harvey Mudd College in 1991 and a Ph.D. in Electrical Engineering from UCSD, in 1999. He was with the Math Sciences Research center at Lucent Technologies in 2000, and has been in the Information Processing Group at the Jet Propulsion Laboratory since 2001. His interests are in information and communication theory, parameter estimation, and constrained modulation. His work at JPL has focused on the design and implementation of deep-space optical communications systems.

Kamal Oudrhiri is a senior member in the Radio Science Systems Group at NASAs Jet Propulsion Laboratory. As a contract technical manager, Oudrhiri led multi-disciplinaryteams through the design, implementation and delivery of flight hardware to the radio science community. Over the last decade, Oudrhiriserved in key roles on multiple NASA missions: The Mars Exploration Rovers (MER), the International Cassini mission to Saturn,The GRAIL lunar mission and The Mars Science Laboratory (MSL). 7

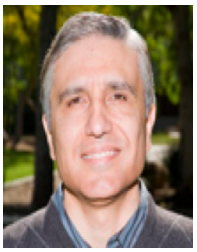

Sami Asmar is the supervisor of JPLs Radio Science Systems Group, the Project Scientist for the GRAIL lunar mission, and an active gravity science co-investigator on US and European planetary missions.